

# Tungsten vs Selenium as a potential source of kilonova nebular emission observed by *Spitzer*

Kenta Hotokezaka,<sup>1,2</sup>★ Masaomi Tanaka,<sup>3,4</sup> Daiji Kato,<sup>5,6</sup> Gediminas Gaigalas<sup>7</sup>

<sup>1</sup>Research Center for the Early Universe, Graduate School of Science, The University of Tokyo, Bunkyo, Tokyo 113-0033, Japan

<sup>2</sup>Kavli IPMU (WPI), UTIAS, The University of Tokyo, Kashiwa, Chiba 277-8583, Japan

<sup>3</sup>Astronomical Institute, Tohoku University, Sendai 980-8578, Japan

<sup>4</sup>Division for the Establishment of Frontier Sciences, Organization for Advanced Studies, Tohoku University, Sendai 980-8577, Japan

<sup>5</sup>National Institute for Fusion Science, 322-6 Oroshi-cho, Toki 509-5292, Japan

<sup>6</sup>Department of Advanced Energy Engineering Science, Kyushu University, Kasuga, Fukuoka 816-8580, Japan

<sup>7</sup>Institute of Theoretical Physics and Astronomy, Vilnius University, Saulėtekio Ave. 3, Vilnius, Lithuania

Accepted XXX. Received YYY; in original form ZZZ

## ABSTRACT

Infrared emission lines arising from transitions between fine structure levels of heavy elements are expected to produce kilonova nebular emission. For the kilonova in GW170817, strong emission at  $4.5\ \mu\text{m}$  at late times was detected by the *Spitzer* Space Telescope but no source was detected at  $3.6\ \mu\text{m}$ . This peculiar spectrum indicates that there exist strong line emitters around  $4.5\ \mu\text{m}$  and the absence of strong lines around  $3.6\ \mu\text{m}$ . To model the spectrum we prepare a line list based on the selection rules in LS coupling from the experimentally calibrated energy levels in the NIST database. This method enables to generate the synthetic spectra with accurate line wavelengths. We find that the spectrum is sensitive to the abundance pattern whether or not the first r-process peak elements are included. In both cases, the synthetic spectra can match the observed data, leading to two possible interpretations. If the first peak elements are abundant a Se III line dominates the flux. If otherwise, W III with Os III, Rh III, and Ce IV can be the main sources. Observing nebular spectra for the future kilonovae in a wider wavelength range can provide more conclusive elemental identification.

**Key words:** transients: neutron star mergers

## 1 INTRODUCTION

The origin of r-process elements is a long-standing problem in astrophysics (Burbidge et al. 1957; Cameron 1957). Neutron star mergers have been considered as promising sites of r-process nucleosynthesis (Lattimer & Schramm 1974). A neutron star merger, GW170817, was accompanied by an uv-optical-infrared counterpart referred to as ‘kilonova’ or ‘macronova’ (Abbott et al. 2017). The light curve and spectrum indicate that a large amount of r-process elements is produced in this event (see Metzger 2017; Nakar 2020; Margutti & Chornock 2021, for reviews). The amount of the ejecta together with the event rate suggests that neutron star mergers can provide all the r-process elements in the Galaxy (e.g. Hotokezaka et al. 2018; Rosswog et al. 2018).

Currently, strontium (Sr, atomic number  $Z = 38$ ) seems only the element that is identified from a structure like the P Cygni profile in the early kilonova spectra (Watson et al. 2019 and see also Domoto et al. 2021; Gillanders et al. 2022 but also Perego et al. 2022 for an alternative explanation by He). Apart from Sr, the spectral evolution implies the existence of lanthanides (Tanaka et al.

2017; Kasen et al. 2017; Kawaguchi et al. 2018; Wollaeger et al. 2021) because the opacity is sensitive to their abundances (Barnes & Kasen 2013; Tanaka & Hotokezaka 2013; Fontes et al. 2020).

Kilonova nebular emission at the later times imprints information on atomic species synthesized in neutron star mergers. A fraction of nebular emission is expected to be radiated in infrared wavelengths through forbidden lines (Hotokezaka et al. 2021). The *Spitzer* Space Telescope observed the nebular phase of the kilonova in GW170817 at 43 and 74 days (Kasliwal et al. 2022). Strong emission was indeed detected at the  $4.5\ \mu\text{m}$  band (Villar et al. 2018; Kasliwal et al. 2022), of which the amount of energy radiated in this band is about ten per cent of the total radioactive heating (e.g., Hotokezaka & Nakar 2020). On the contrary, upper limits were obtained at the  $3.6\ \mu\text{m}$  band at both epochs, indicating that there exist strong emission lines around  $4.5\ \mu\text{m}$  and the absence of such lines in the  $3.6\ \mu\text{m}$  band. Although the physical conditions of kilonova nebulae are studied in the literature (Hotokezaka et al. 2021; Pognan et al. 2022b) any attempts to model this peculiar emission feature have not yet been made because of the lack of atomic data with accurate line wavelengths. In this *Letter*, we present the synthetic spectra of kilonova nebular emission in the wavelength range observed by *Spitzer* including most of the relevant atomic species.

★ E-mail: kentah@gcc.u-tokyo.ac.jp

In §2, we estimate the infrared emission of fine structure lines of heavy elements. In §3, we produce a line list from the energy levels in the NIST database and present the synthetic spectra of kilonova nebular emission. In §4, we conclude our findings.

## 2 FINE STRUCTURE EMISSION LINES

The energy scale of fine structure splitting of heavy elements is typically  $\sim 0.01 - 1$  eV. Because the optical depth of the kilonova ejecta to bound-bound transitions is  $\lesssim 0.1$  at 40 days at wavelengths longer than near infrared (e.g. Tanaka et al. 2020; Pognan et al. 2022a), emission lines arising from transitions between fine structure levels are expected to freely escape on this time scale. The strength of each line is determined by the level population and radiative transition rate. The rate of a magnetic dipole (M1) transition from an upper level  $u$  to a lower level  $l$  that satisfy the M1 selection rules in LS coupling<sup>1</sup> is given by (Pasternack 1940; Shortley 1940; Bahcall & Wolf 1968)

$$A_{ul} = 1.3 \text{ s}^{-1} \left( \frac{\lambda_{ul}}{4 \mu\text{m}} \right)^{-3} f(J, L, S), \quad (1)$$

where  $\lambda_{ul}$  is the line wavelength and  $f(J, L, S)$  is an algebraic factor depending on the total angular momentum  $J$ , total orbital angular momentum  $L$ , and total spin angular momentum  $S$  of the upper level in units of  $\hbar$ . LS coupling is known as a good approximation only for light elements. However, we find that this formula is accurate to 10 per cent even for a transition rate of Ac III ( $Z=89$ , Kramida et al. 2021). The collisional deexcitation rate coefficient is given by

$$\langle \sigma v \rangle_{ul} = \frac{8.63 \cdot 10^{-8} \Omega_{ul}(T_e)}{\sqrt{T_{e,4}}} \frac{\Omega_{ul}(T_e)}{g_u} \text{ cm}^3 \text{ s}^{-1}, \quad (2)$$

where  $\Omega_{ul}(T_e)$  is the collision strength,  $g_u$  is the statistical weight of the upper level, and  $T_{e,4}$  is the electron temperature in units of  $10^4$  K. Comparing  $A_{ul}$  and  $\langle \sigma v \rangle_{ul}$  one finds a critical density of  $\sim 10^7 \text{ cm}^{-3} (g_u/\Omega_{ul})(T_e/3000 \text{ K})^{1/2} (\lambda_{ul}/4 \mu\text{m})^{-3}$ . Because the electron density of the kilonova ejecta at 40 days is  $n_e \sim 10^5 - 10^6 \text{ cm}^{-3}$  M1 radiative decay is typically faster than collisional deexcitation suggesting that the ground levels are overpopulated compared to the expected values from the thermal distribution. Therefore strong lines in infrared wavelengths are expected to arise from transitions between fine-structure levels in the ground terms.

Doubly ionized selenium (Se III,  $Z = 34$ ) and tungsten (W III,  $Z = 74$ ) are good examples of ions having fine structure transitions in their ground term in the *Spitzer*  $4.5 \mu\text{m}$  band. Figure 1 shows the fine structure levels of the ground terms  $^3P_J$  for Se III and  $^5D_J$  for W III (Kramida et al. 2021) with arrows depicting M1 transitions. Also shown are the radiative transition rates derived from equation 1 and their wavelengths. Since ions with the ground term of  $^5D_J$  have five fine structure levels they are expected to be possible infrared line emitters (Berrington 1995). W III indeed has two emission lines at  $4.432$  and  $4.535 \mu\text{m}$  from the first and the second excited levels.

At the densities lower than the critical density, the emission rate is determined by collisional excitation rather than the radiative transition rates. For a fine structure line  $u \rightarrow l$ , the emission rate

<sup>1</sup> The selection rules in LS coupling are (1)  $\Delta J = 0, \pm 1$  (except  $0 \leftrightarrow 0$ ), (2) no parity change, (3) no change in electron configuration, (4)  $\Delta S = \Delta L = 0$  and  $\Delta J = \pm 1$ .

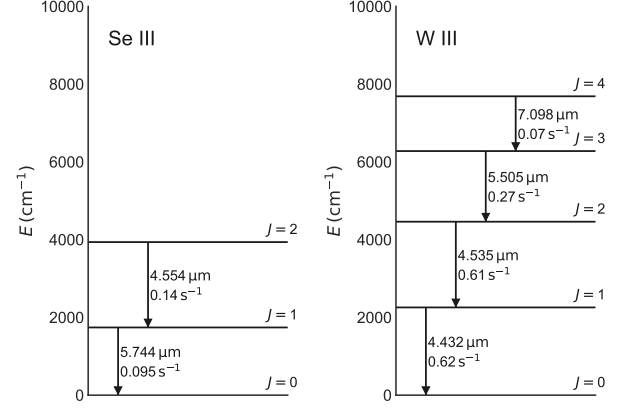


**Figure 1.** Energy-level diagram of the fine structure of the ground terms of Se III  $4p^2 \ ^3P_J$  ( $Z = 34$ ) and W III  $5d^4 \ ^5D_J$  ( $Z = 74$ ). Arrows depict M1 transitions with radiative transition rates and transition wavelengths.

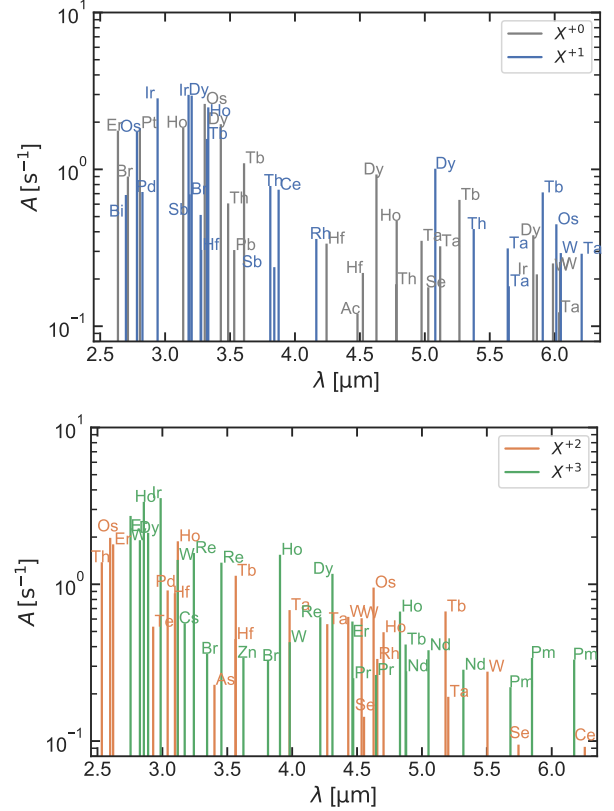


**Figure 2.** M1 transitions between fine-structure levels of the ground terms in the range of  $2.5 - 6.3 \mu\text{m}$ . Ions,  $X^{+0} - X^{+3}$ , for atomic numbers  $Z \geq 30$  are shown.

per ion is approximated by the collisional excitation rate from the ground level to  $u$ :

$$\epsilon_{ul} \approx \frac{0.0863}{\sqrt{T_{e,4}}} \frac{\Omega_{u0}}{g_0} \frac{n_e}{10^6 \text{ cm}^{-3}} e^{-E_{u0}/kT_e} \text{ s}^{-1}, \quad (3)$$

where  $E_{u0}$  is the excitation energy of level  $u$  from the ground level.

For instance, the total luminosity in [W III]  $4.43 \mu\text{m}$  and [W

III] 4.54  $\mu\text{m}$  for  $T_e \sim 3500$  K is estimated by

$$L_{4.5\mu\text{m}}(\text{W III}) \sim 5 \cdot 10^{37} \text{ erg/s} \frac{\Omega_{u0} n_e}{10^6 \text{ cm}^{-3}} \frac{M_{\text{ej}}}{0.05 M_{\odot}} \frac{X_W}{0.004}, \quad (4)$$

where  $M_{\text{ej}}$  is the total ejecta mass and  $X_W$  is the mass fraction of W III including all the isotopes existing at a given epoch. It is possible that this luminosity accounts for a large fraction of the observed luminosity in the 4.5  $\mu\text{m}$ -band at 43 days of  $\Delta\nu L_{\nu} \sim 2 \cdot 10^{38}$  erg/s (Kasliwal et al. 2022) and  $7 \cdot 10^{37}$  erg/s (Villar et al. 2018).

In this paper, we assume that dust grains are absent in the kilonova ejecta, and therefore, the infrared emission is entirely produced by atomic emission lines. This assumption is supported by Takami et al. (2014), where it is shown that the dust formation in the ejecta is unlikely to occur unless light elements such as carbon are abundant (see also Gall et al. 2017; Villar et al. 2018, in the context of GW170817).

### 3 SYNTHETIC NEBULAR SPECTRUM FOR SPITZER OBSERVATION

In order to refine the rough estimates given in the previous section we collected the experimentally calibrated energy levels that are available in the NIST database (Kramida et al. 2021) for neutral to triply ionized ions of all the relevant atomic species and produced a line list by using the M1 selection rules in the single configuration approximation. In particular, here we restrict ourselves to the LS coupling scheme because the NIST database uses LS terms to represent energy levels for most ions relevant to this work. In addition to the NIST data, the energy levels of Hf III and Ta III are taken from Malcheva et al. (2009) and Azarov et al. (2003), of which the level identification may not be as accurate as the NIST data. The transition rate of each line is assigned according to the formula 1. On one hand, our line list is not necessarily complete because it is limited by the availability of energy levels in the NIST database and lines existing in intermediate coupling are not included. On the other hand, this method guarantees good accuracy of wavelengths. Therefore it enables to generate synthetic spectra, which are useful for comparison to observed data. Figure 2 shows the fine-structure lines of the ground terms of  $X^{+0} - X^{+3}$  with  $Z \geq 30$  in 2.5–6.3  $\mu\text{m}$ .

Other key ingredients in the modelings are collision strengths,  $\Omega_{ul}$ , which are generally large  $\mathcal{O}(1)$  for fine structure transitions. In this work we use an atomic structure code HULLAC (Bar-Shalom et al. 2001) to compute the collision strengths for transitions between levels of ground terms, which are the most relevant ones. Otherwise, we assume  $\Omega_{ul} = 1$ .

Since the r-process abundance pattern of the ejecta in GW170817 is under debate, here we consider two sets of the abundance patterns: (1) the solar r-process abundance pattern (Goriely 1999) including the first r-process peak elements (atomic mass numbers  $A \geq 69$ ; model\_1st) and (2) that excluding the first peak ( $A \geq 88$ ; model\_2nd-3rd). In the former case,  $\sim 70\%$  of the mass is in the first peak elements. We assume the ejecta properties of  $M_{\text{ej}} = 0.05 M_{\odot}$ ,  $v_{\text{ej}} = 0.1c$ ,  $\chi_e = 1$ , and  $T_e = 2000$  K for model\_1st, where  $v_{\text{ej}}$  and  $\chi_e$  are the mean ejecta velocity and free electron fraction. For model\_2nd-3rd, we use  $M_{\text{ej}} = 0.05 M_{\odot}$ ,  $v_{\text{ej}} = 0.07c$ ,  $\chi_e = 2$ , and  $T_e = 3500$  K. The two examples of the spectra with the different ionization stages are considered: (i)  $X^{+1} \& X^{+2}$  and (ii)  $X^{+2} \& X^{+3}$ . For demonstration purposes, the fractions of the two ionization stages are assumed to be equal in both cases. For a given  $n_e$  and  $T_e$ , the level population of each ion is solved with a similar method employed in Hotokezaka et al. (2021).

Figure 3 shows the emission-line spectra at 43 days. It is somewhat surprising that both model\_1st and model\_2nd-3rd can match the *Spitzer* detection and upper limit (see also table 1) except model\_2nd-3rd ( $X^{+1} \& X^{+2}$ ) while their emission spectra are clearly different outside the *Spitzer*-bands. In model\_1st, a single line, [Se III] 4.55  $\mu\text{m}$ , completely dominates the flux at the 4.5  $\mu\text{m}$  band. This is simply because Se is the most abundant atomic species. If this is the case, an even stronger emission line [Se III] 5.74  $\mu\text{m}$  must exist. Although As III, Br II, and Br IV, which are next to Se in the periodic table, have lines in the 3.6  $\mu\text{m}$  band their fluxes are sufficiently small because of their lower abundances. In model\_2nd-3rd, W III, Ce IV, Rh III, and Os III can produce the observed 4.5  $\mu\text{m}$  flux. However, Sb II overproduces emission in the 3.6  $\mu\text{m}$  band compared to the observed limit. This suggests that most of Sb atoms are in highly ionized states, e.g., Sb III.

The observed luminosity in the 4.5  $\mu\text{m}$  band at 43 days is  $\sim 10^{38}$  erg/s, which is a few per cent of or even comparable to the total luminosity expected from  $\beta$ -decay thermalization (Waxman et al. 2019; Kasen & Barnes 2019; Hotokezaka & Nakar 2020). Such a high radiative efficiency in mid-infrared indicates that the electron temperature in this epoch is low,  $T_e \lesssim 5000$  K, otherwise the thermal energy is predominantly radiated at the shorter wavelengths. We estimate that the total luminosities in M1 lines at 43 days are  $\sim 5 \cdot 10^{38}$  erg/s for model\_1st and  $\sim 2 \cdot 10^{39}$  erg/s for model\_2nd-3rd. In the case of model\_1st, the luminosity exceeds the total heating rate expected from the adopted abundances. This indicates that the relative abundances of the first peak elements are not as large as the solar r-process abundances even if Se dominates the 4.5  $\mu\text{m}$  flux.

It is also important to note that  $\sim 50\%$  of W atoms at 43 days are in radioactive isotopes  $^{185}\text{W}$  and  $^{188}\text{W}$ , of which half-lives are 75.1 and 69.8 days, respectively. In model\_2nd-3rd, therefore, the relative strength of the emission around 4.5  $\mu\text{m}$  is expected to decrease by a factor of  $\sim 2$  after these isotopes have disappeared. The decay chain  $^{188}\text{W} \rightarrow ^{188}\text{Re} \rightarrow ^{188}\text{Os}$  releases  $\sim 900$  keV in  $\beta$  radiation, which means that W itself is an energy and ionizing source. Therefore, the emission of W and Os may be enhanced if the light and heavy elements are spatially separated in the ejecta and  $\beta$  electrons are locally confined by magnetic fields (Barnes et al. 2016; Waxman et al. 2019). On the contrary, there are no radioactive elements for  $69 \leq A \leq 88$  with a half-life of 10–100 days, thereby the emission of Se may be strongly suppressed if such inhomogeneous heating exists.

Our choices of the ionization stages are motivated by Hotokezaka et al. (2021) and Pognan et al. (2022b), where ionization in the kilonova nebular phase is studied. Hotokezaka et al. (2021) showed that the dielectronic recombination rates of Nd ions are  $\gtrsim 10^{-10} \text{ cm}^3 \text{ s}^{-1}$ , which are significantly larger than the radiative recombination rates. As a result, they found that Nd atoms are in Nd II and Nd III around 40 days. If the recombination rate is lower  $\sim 10^{-11} \text{ cm}^3 \text{ s}^{-1}$ , the typical ionization stage is  $X^{+2}$  or  $X^{+3}$  (Pognan et al. 2022b). The dielectronic recombination rates of Se and W ions are rather similar to Nd at the nebular temperatures (Sterling & Witthoeft 2011; Preval et al. 2019). Therefore we expect that Se and W at 43 days are predominantly in the singly and doubly ionized ions. If this is the case and model\_2nd-3rd is correct, emission lines of [Os III] 2.60  $\mu\text{m}$ , [Os II] 2.78  $\mu\text{m}$ , [Os II] 6.01  $\mu\text{m}$ , and [W II] 6.05  $\mu\text{m}$  may produce observable features.

We now turn to discuss the caveats in our analysis. Our line list is not necessarily complete because it contains only M1 transitions within the single configuration approximation, i.e., most lines in our list are those arising from transitions between fine structure levels of a given LS term. This is no longer a good approximation for heavy

**Table 1.** *Spitzer* AB magnitude of the kilonova GW170817 at 43 days.

Wavelength	model_1st, $X^{+1,+2}$	model_1st, $X^{+2,+3}$	model_2nd-3rd, $X^{+1,+2}$	model_2nd-3rd, $X^{+2,+3}$	Observed <sup>(1)</sup>	Observed <sup>(2)</sup>
3.6 $\mu\text{m}$	24.6	24.5	22.4	23.8	> 23.21	> 23.3
4.5 $\mu\text{m}$	22.7	22.8	22.8	22.7	$21.88 \pm 0.04 (\pm 0.05)$	$22.9 \pm 0.3$

(1) Kasliwal et al. (2022). The  $3\sigma$  upper limit at 3.6  $\mu\text{m}$  is shown. The systematic error is shown in the parenthesis.

(2) Villar et al. (2018). The  $3\sigma$  upper limit at 3.6  $\mu\text{m}$  is shown. The error of the 4.5  $\mu\text{m}$  detection is dominated by systematic uncertainties.

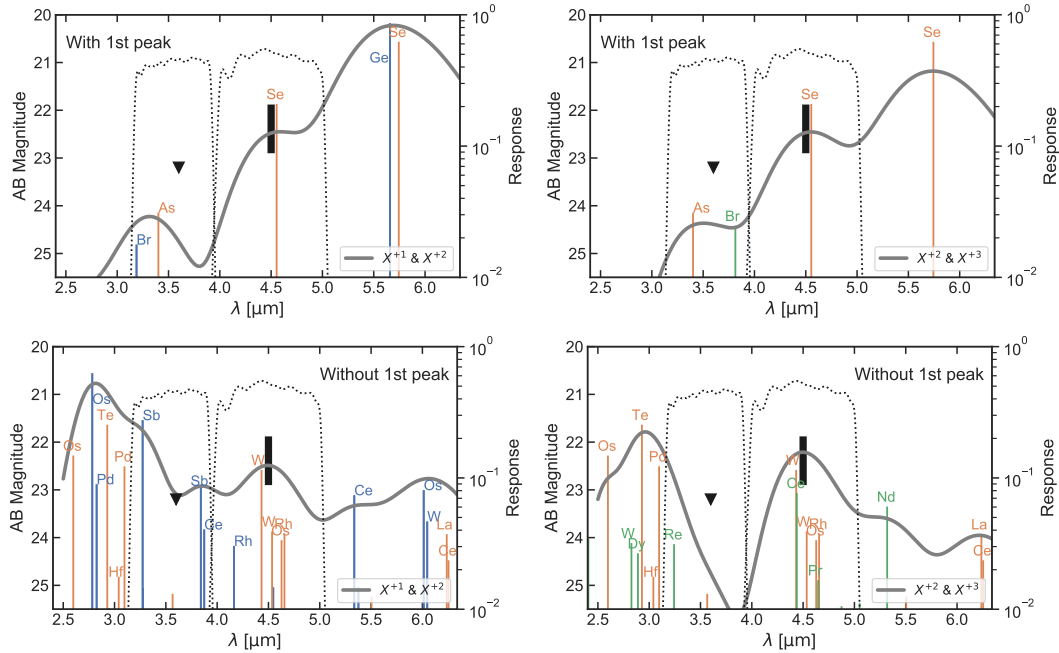


**Figure 3.** Synthetic spectra for the kilonova in GW170817 at 43 days. The solar r-process abundance pattern with the first peak elements ( $A \geq 69$ , model\_1st) and that without the first peak elements ( $A \geq 88$ , model\_2nd-3rd) are used in the *upper* and *lower* panels. The ionization fractions are assumed to be equal for  $X^{+1}$  and  $X^{+2}$  (left) and for  $X^{+2}$  and  $X^{+3}$  (right). The total flux is obtained by adding the contributions of all lines, where the Doppler-shifted line profile is assumed to be a Gaussian in frequency space with a broadening parameter  $v_{ej} = 0.1c$  and  $0.07c$  for model\_1st and model\_2nd-3rd, respectively. Blue, orange, and green vertical lines indicate the wavelength of each line in the rest frame for  $X^{+1}$ ,  $X^{+2}$ , and  $X^{+3}$ , respectively. The height of the vertical lines corresponds to the total flux in a line divided by  $v_{ej}/\lambda_{ul}$ . Also depicted are the *Spitzer*-4.5  $\mu\text{m}$  detection, the 3.6  $\mu\text{m}$  upper limit, and the spectral responses as a vertical bar, a triangle, and dotted lines. (<https://irsa.ipac.caltech.edu/data/SPITZER/docs/irac/calibrationfiles/spectralresponse/>). The bar indicates the range of the AB magnitudes estimated by the two different groups (Kasliwal et al. 2022; Villar et al. 2018).

elements, where two types of mixing are important; (i) the mixing between different final and intermediate terms within the same configuration and (ii) the mixing between different configurations. The former effect starts to appear for elements around the second r-process peak,  $Z \gtrsim 50$ . The latter is important for heavier elements, e.g.,  $Z \gtrsim 74$ . Note, however, that fine structure transitions are usually less sensitive to these effects compared to other transitions such as optical lines. Our list is also limited by the availability of energy levels in the NIST database. For example, Ir III, Pt III, and Au III as well as elements of  $Z \geq 91$  are not contained. In such cases, one must rely on atomic structure codes to infer the energy levels. For instance, Gillanders et al. (2021) studied the energy levels of Pt III and Au III by using GRASP<sup>0</sup> and showed that there are no emission lines in 3  $\mu\text{m}$  to 5  $\mu\text{m}$  arising from the transitions between the lower-lying energy levels. Nevertheless, we should keep in mind that there can be additional lines.

Another caveat is that we do not include electric dipole transitions (E1). This is a reasonable assumption for the typical ion, of which the energy scale of E1 transitions is usually larger than

1 eV. However, some lanthanide ions, e.g. Ce II and Tb II, have E1 transition lines in mid-infrared. Including these lines may also affect our conclusion. Finally, we use collision strengths computed with HULLAC, which are not as accurate as those with the R-matrix method. For the transitions between the levels within the ground term of Se III and that between the ground and first excited level of W IV, we find that our collision strengths agree within a factor of 2 with those presented in Sterling et al. (2017) and Ballance et al. (2013), where the R-matrix method is used. However, for Te III and excitation to the higher levels of W IV, our collision strengths can be lower by a factor of  $\sim 5$  (Madonna et al. 2018; Ballance et al. 2013). This difference may be due to the fact that we do not include resonant excitation. Therefore, the relative line intensities may change if more accurate collision strengths are used.

#### 4 CONCLUSION

We study the kilonova nebular emission in the range of 3 – 5  $\mu\text{m}$ , where the *Spitzer* Space Telescope observed the kilonova in



GW170817 at 43 and 74 days (Kasliwal et al. 2022). We produce an M1 line list for  $X^{+0}$ – $X^{+3}$  from the energy levels available in the NIST database (Kramida et al. 2021) by using the M1 selection rules in LS coupling under the single configuration approximation. This method enables to generate the synthetic spectra in infrared with accurate wavelengths. In the range of  $3 - 5 \mu\text{m}$  our line list contains  $\sim 100$  fine structure lines. With this list, the synthetic nebular spectra with two sets of the abundance patterns with or without the first r-process peak elements are computed for two different ionization states,  $X^{+1}$  &  $X^{+2}$  and  $X^{+2}$  &  $X^{+3}$ . Our findings and predictions are the followings:

- The kilonova nebular spectrum in mid-infrared is sensitive to the abundance pattern whether the first r-process peak elements are included or not. Nevertheless, the synthetic spectra can match the observed  $4.5 \mu\text{m}$  detection and  $3.6 \mu\text{m}$  upper limit in both cases.
- If the first r-process peak elements are abundant, [Se III]  $4.55 \mu\text{m}$  completely dominates the flux at the  $4.5 \mu\text{m}$  band because Se is the most abundant atomic species. In this case a strong emission feature due to [Se III]  $5.74 \mu\text{m}$  must exist, which may be accompanied by [Ge II]  $5.66 \mu\text{m}$ .
- If the ejecta is dominated by elements beyond the first peak, W III, Os III, Rh II, Rh III, and Ce IV can produce an emission feature around  $4.5 \mu\text{m}$ . Combining their emission lines can account for the observed flux with the solar r-process abundances.
- If W III and Os III are the main sources of the observed flux we expect that [Os III]  $2.60 \mu\text{m}$ , [Os II]  $2.78 \mu\text{m}$ , [Os II]  $6.01 \mu\text{m}$ , and [W II]  $6.05 \mu\text{m}$  may produce observable features.
- In the case without the first peak elements, some singly ionized ions, e.g., Sb II and Ce II, have strong lines around  $3.6 \mu\text{m}$ . The observed upper limit implies that these atoms are likely in the higher ionization states.

If a kilonova is successfully identified within  $\sim 100 \text{ Mpc}$  in the future, the James Webb Space Telescope will be able to provide the nebular spectra with a better quality across a wider wavelength range. With such data more detailed analysis can be done. In order to extract more information about the elemental abundances and the ejecta properties, more atomic data, e.g., collision strengths and complete line lists (Gaigalas et al. 2019; Gillanders et al. 2021; Silva et al. 2022), as well as sophisticated modelings of the ionization states (Hotokezaka et al. 2021; Pognan et al. 2022b) are needed.

## ACKNOWLEDGMENTS

We thank N. Domoto, K. Kawaguchi, and Y. Tarumi for useful discussion and comments. We also thank M. Busquet for the generous support on the HULLAC code. This work was supported by Japan Society for the Promotion of Science (JSPS) Early-Career Scientists Grant Number 20K14513, Grant-in-Aid for Scientific Research from JSPS (20H05639, 20H00158, 19H00694, 21H04997), and MEXT (17H06363).

## DATA AVAILABILITY

The data presented this article will be shared on request to the corresponding author.

## REFERENCES

- Abbott B. P., et al., 2017, *ApJ*, **848**, L12  
 Azarov V. I., Tchchang-Brillet W. Ü. L., Wyart J. F., Meijer F. G., 2003, *Phys. Scr.*, **67**, 190

- Bahcall J. N., Wolf R. A., 1968, *ApJ*, **152**, 701  
 Ballance C. P., Loch S. D., Pindzola M. S., Griffin D. C., 2013, *Journal of Physics B Atomic Molecular Physics*, **46**, 055202  
 Bar-Shalom A., Klapisch M., Oreg J., 2001, *J. Quant. Spectrosc. Radiative Transfer*, **71**, 169  
 Barnes J., Kasen D., 2013, *ApJ*, **775**, 18  
 Barnes J., Kasen D., Wu M.-R., Martínez-Pinedo G., 2016, *ApJ*, **829**, 110  
 Berrington K. A., 1995, *A&AS*, **109**, 193  
 Burbidge E. M., Burbidge G. R., Fowler W. A., Hoyle F., 1957, *Reviews of Modern Physics*, **29**, 547  
 Cameron A. G. W., 1957, *PASP*, **69**, 201  
 Domoto N., Tanaka M., Wanajo S., Kawaguchi K., 2021, *ApJ*, **913**, 26  
 Fontes C. J., Fryer C. L., Hungerford A. L., Wollaeger R. T., Korobkin O., 2020, *MNRAS*, **493**, 4143  
 Gaigalas G., Kato D., Rynkun P., Radžiūtė L., Tanaka M., 2019, *ApJS*, **240**, 29  
 Gall C., Hjorth J., Rosswog S., Tanvir N. R., Levan A. J., 2017, *ApJ*, **849**, L19  
 Gillanders J. H., McCann M., Sim S. A., Smartt S. J., Ballance C. P., 2021, *MNRAS*, **506**, 3560  
 Gillanders J. H., Smartt S. J., Sim S. A., Bauswein A., Goriely S., 2022, arXiv e-prints, p. arXiv:2202.01786  
 Goriely S., 1999, *A&A*, **342**, 881  
 Hotokezaka K., Nakar E., 2020, *ApJ*, **891**, 152  
 Hotokezaka K., Beniamini P., Piran T., 2018, *International Journal of Modern Physics D*, **27**, 1842005  
 Hotokezaka K., Tanaka M., Kato D., Gaigalas G., 2021, *MNRAS*, **506**, 5863  
 Kasen D., Barnes J., 2019, *ApJ*, **876**, 128  
 Kasen D., Metzger B., Barnes J., Quataert E., Ramirez-Ruiz E., 2017, *Nature*, **551**, 80  
 Kasliwal M. M., et al., 2022, *MNRAS*, **510**, L7  
 Kawaguchi K., Shibata M., Tanaka M., 2018, *ApJ*, **865**, L21  
 Kramida A., Yu. Ralchenko Reader J., and NIST ASD Team 2021, NIST Atomic Spectra Database (ver. 5.9), [Online]. Available: <https://physics.nist.gov/asd> [2017, April 9]. National Institute of Standards and Technology, Gaithersburg, MD.  
 Lattimer J. M., Schramm D. N., 1974, *ApJ*, **192**, L145  
 Madonna S., et al., 2018, *ApJ*, **861**, L8  
 Malcheva G., et al., 2009, *MNRAS*, **396**, 2289  
 Margutti R., Chornock R., 2021, *ARA&A*, **59**  
 Metzger B. D., 2017, *Living Reviews in Relativity*, **20**, 3  
 Nakar E., 2020, *Phys. Rep.*, **886**, 1  
 Pasternack S., 1940, *ApJ*, **92**, 129  
 Perego A., et al., 2022, *ApJ*, **925**, 22  
 Pognan Q., Jerkstrand A., Grumer J., 2022a, arXiv e-prints, p. arXiv:2202.09245  
 Pognan Q., Jerkstrand A., Grumer J., 2022b, *MNRAS*, **510**, 3806  
 Preval S. P., Badnell N. R., O’Mullane M. G., 2019, *Journal of Physics B Atomic Molecular Physics*, **52**, 025201  
 Rosswog S., Sollerman J., Feindt U., Goobar A., Korobkin O., Wollaeger R., Fremling C., Kasliwal M. M., 2018, *A&A*, **615**, A132  
 Shortley G. H., 1940, *Physical Review*, **57**, 225  
 Silva R. F., Sampaio J. M., Amaro P., Flörs A., Martínez-Pinedo G., Marques J. P., 2022, *Atoms*, **10**, 18  
 Sterling N. C., Witthoeft M. C., 2011, *A&A*, **529**, A147  
 Sterling N. C., Madonna S., Butler K., García-Rojas J., Mashburn A. L., Morisset C., Luridiana V., Roederer I. U., 2017, *ApJ*, **840**, 80  
 Takami H., Nozawa T., Ioka K., 2014, *ApJ*, **789**, L6  
 Tanaka M., Hotokezaka K., 2013, *ApJ*, **775**, 113  
 Tanaka M., et al., 2017, *PASJ*, **69**, 102  
 Tanaka M., Kato D., Gaigalas G., Kawaguchi K., 2020, *MNRAS*, **496**, 1369  
 Villar V. A., et al., 2018, *ApJ*, **862**, L11  
 Watson D., et al., 2019, *Nature*, **574**, 497  
 Waxman E., Ofek E. O., Kushnir D., 2019, *ApJ*, **878**, 93  
 Wollaeger R. T., et al., 2021, *ApJ*, **918**, 10

This paper has been typeset from a  $\text{\LaTeX}$  file prepared by the author.